IEEE Photonics Journal
An IEEE Photonics Society Publication

Open Access

Integration and Application of Microlens Arrays Within Heads-Up Displays

Volume 10, Number 6, December 2018

Weicheng Yan
Xian Jin
Hongbae S. Park
Ashli Le Blanc
Hamid Abdollahi
Boris Stoeber
Jonathan F. Holzman

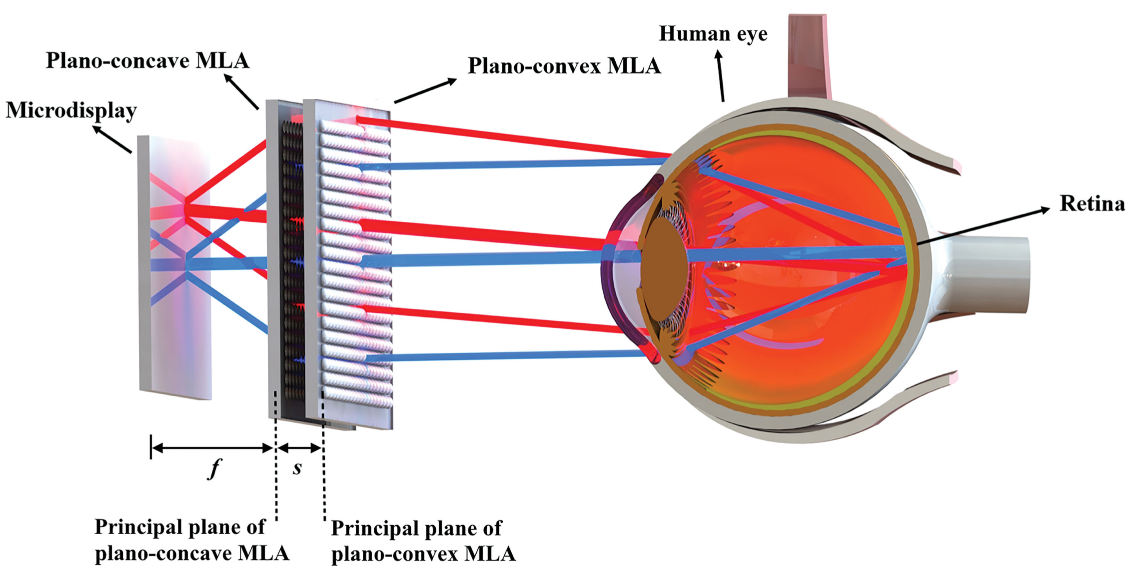

DOI: 10.1109/JPHOT.2018.2876386

Integration and Application of Microlens Arrays Within Heads-Up Displays

Weicheng Yan,[1] Xian Jin,[1] Hongbae S. Park,[2] Ashli Le Blanc,[1] Hamid Abdollahi,[3] Boris Stoeber ,[2,4] and Jonathan F. Holzman [1]

[1]Integrated Optics Laboratory, School of Engineering, University of British Columbia, Kelowna, BC V1V 1V7, Canada
[2]Department of Electrical and Computer Engineering, University of British Columbia, Vancouver, BC V6T 1Z4, Canada
[3]Intel Corporation, Vancouver, BC V5X 4V2, Canada
[4]Department of Mechanical Engineering, University of British Columbia, Vancouver, BC V6T 1Z4, Canada

DOI:10.1109/JPHOT.2018.2876386

Manuscript received July 27, 2018; revised September 26, 2018; accepted October 13, 2018. Date of publication October 16, 2018; date of current version October 29, 2018. This research was funded by the Natural Sciences and Engineering Research Council of Canada (NSERC, RGPIN-341487-12) and the Mitacs Accelerate Program (BC-ISED IT11019). Corresponding author: Jonathan F. Holzman (e-mail: jonathan.holzman@ubc.ca).

Abstract: The proposed work targets a fundamental challenge in heads-up display technology—in that such displays must bring about tight imaging with a flat form factor to support integration within eyewear. A Gabor superlens, being coupled plano-concave and plano-convex microlens arrays (MLAs), is developed to meet this challenge. The MLAs are designed and optimized, via tradespace analyses and ray-based simulations, and then formed with a specialized fabrication process. The process applies plasma pretreatment to the substrate followed by dispensing, curing, and casting of microlenses on the substrate to realize arrays with the necessary diameters and radii of curvature. The plano-concave and plano-convex MLAs are coupled to form the superlens, which is packaged with a baffle and microdisplay to function as the heads-up display. Ray-based simulations and experimental characterizations are carried out on the modulation transfer function of the display to define its resolution. It is found that the superlens can bring about strong imaging performance—with a resolution of up to 30 cycles/mm—as well as the tight imaging and flat form factor that are needed for emerging heads-up display technologies.

Index Terms: Displays, lenses, microarchitecture, optical imaging, optical polymers.

1. Introduction

Heads-Up display technology has revolutionized virtual reality and augmented reality systems [1], [2]. Such technology projects the image of a microdisplay into the human eye to display real-time analytics and has been very successful for realizations in helmets and goggles. However, there is growing demand to integrate heads-up displays within contemporary eyewear, which is far more compact, and this has revealed a fundamental challenge for optical design.

The design of a heads-up display witnesses conflicting aims when implemented in eyewear. Its optics must enable tight imaging, to capture and display an image of the nearby microdisplay to the relaxed eye, being focused at infinity, and the optics must have a sufficiently flat form factor, to facilitate compact integration within eyewear [3]. The challenge arises because a lens with high curvature is needed to capture the nearby image and project it as a virtual image at infinity, and

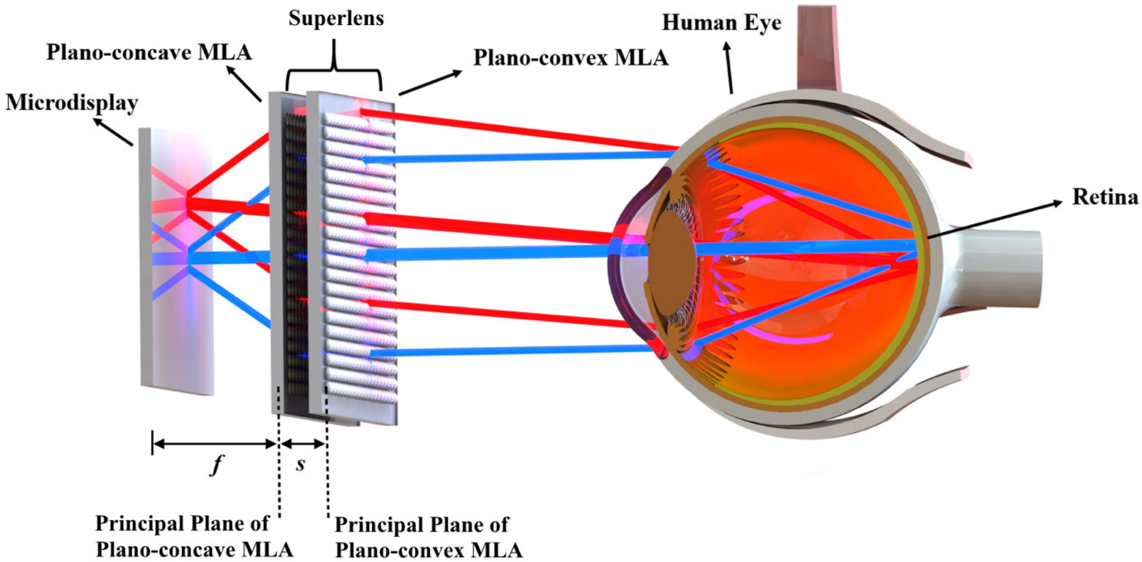

Fig. 1. | **Schematic of the heads-up display's microdisplay and superlens with a human eye.** The superlens is a coupled plano-concave MLA and plano-convex MLA. It displays a virtual image of the microdisplay to the eye and forms an image on the retina. Representative light rays are shown. The baffle, located between the MLAs, is not shown. The design of the human eye was created by Sergey White and was used here with permission.

such a lens has a thick form factor. There is an alternative design that can achieve the tight imaging and flat form factor, however, and it takes the form of a Gabor superlens. The Gabor superlens is a multilayered photonic structure that is named from its analogy to the electronic superlattice [4]–[6]. It is implemented as coupled microlens arrays (MLAs) having offset periodicity. With the appropriate design, the coupled MLAs can exhibit the necessary tight imaging, like a high-curvature lens, and it can do this with a flat form factor [7].

In this work, a superlens is designed, fabricated, and tested for application to heads-up displays. Its design makes use of coupled plano-concave and plano-convex MLAs that achieve tight imaging of the microdisplay with the desired flat form factor [8]. Tradespace analyses [9] and ray-based simulations [10] are used to design the superlens and optimize its parameters. The MLAs for the optimized superlens are then created by a specialized fabrication process that enables precise control over the diameter and radius of curvature of the individual microlenses. The process makes use of a plasma pre-treatment of the glass substrate, to raise its surface energy and increase its wettability to polymer [12], followed by dispensing and curing of polymer microdroplets on the substrate [11]. The arrays of microlenses are used as is, in the form of the plano-convex MLA, or as a mold for casting [13], to form the plano-concave MLA. The plano-concave and plano-convex MLAs are coupled to form the superlens, which is then packaged with a microdisplay and tested as a heads-up display. It is found that the developed superlens can deliver tight imaging performance in a flat form factor—and can meet the demands of future heads-up displays.

2. Parameter Optimization and Ray-Based Simulation

A schematic of the proposed heads-up display is shown in Fig. 1. It includes a microdisplay, superlens, and human eye. The microdisplay (Sony ECX336A) has an active area of 5.0 mm by 3.1 mm. The superlens is a plano-concave MLA coupled to a plano-convex MLA. The superlens uses two confocal MLAs though, in general, two or more MLAs could be used. This has the superlens be as thin and compact as possible. For the same reason, plano-concave and plano-convex MLAs are used. The negative and positive focal lengths of such MLAs are overlapped when they are placed in the needed confocal arrangement, and this yields a smaller separation between MLAs in comparison to that achieved by two plano-convex MLAs. (Although it is not shown in this work, the coupled plano-concave and plano-convex MLAs have an additional advantage in that they yield a larger eyebox, being the volume within which the collimated light rays from the entire microdisplay can be viewed by the relaxed eye.) The plano-concave MLA has microlenses with a pitch, radius of curvature, and focal length denoted by p_{cc}, R_{cc}, and f_{cc}, respectively, while the plano-convex MLA has microlenses with a pitch, radius of curvature, and focal length denoted by p_{cv}, R_{cv}, and f_{cv}, respectively. The effective focal length between the microdisplay and principal plane of the plano-concave MLA is denoted by f. The separation between the principal planes of the MLAs is denoted by s.

The above parameters of the coupled MLAs are critical to the functioning of the superlens, and such functionality can be defined via ray transfer matrices [14], [15]. It can be shown that the coupled MLAs can function as a superlens, and form a virtual image at infinity, only when their parameters obey the following relationships [18]:

$$f = \frac{(s - f_{cv})\, f_{cc}}{s - f_{cc} - f_{cv}} = \frac{p_{cv}}{p_{cv} - p_{cc}} f_{cc}, \tag{1}$$

$$\frac{p_{cv}}{p_{cc}} = \frac{s - f_{cv}}{f_{cc}}, \tag{2}$$

$$s = \frac{f\, f_{cc}}{f - f_{cc}} + f_{cv}, \tag{3}$$

$$p_{cv} = p_{cc} \frac{f}{f - f_{cc}}. \tag{4}$$

The physicality of these equations can be seen by considering each microlens in the plano-concave MLA to be paired with a microlens in the plano-convex MLA and by visualizing the pair of plano-concave and plano-convex microlenses at the centre of the MLAs to be centred with each other along the optical axis. We then note from (4) that the pitch of the plano-concave MLA, p_{cc}, must differ from the pitch of the plano-convex, p_{cv}, to yield physical solutions for the remaining variables. Given the differing pitches, the offsets between the centres of the paired plano-concave and plano-convex microlenses will grow in proportion to the radial displacement off the optical axis. This pattern of (roughly) radially-symmetric and increasing offsets between paired microlenses establishes the desired convergence or divergence of light rays as they pass through the MLAs—in the same manner that the radially-symmetric curvature of a conventional lens yields convergence or divergence of light rays.

The parameter values for the plano-convex MLA can be assigned first, with consideration only to the ease of fabrication. The pitch and radius of curvature of its microlenses are set at $p_{cv} = 440$ μm and $R_{cv} = 497$ μm, respectively. This gives a focal length of $f_{cv} = 943$ μm for a refractive index of 1.524, being that of the plano-convex polymer microlenses and their underlying 100-μm-thick glass substrate.

The remaining parameter values are assigned by tradespace analyses that map out the relationships in equations (1)–(4) and define values according to three design criteria. The first design criterion relates to the angular field-of-view (FOV_A) of the superlens. It is the span of angles over which the superlens displays an image of the microdisplay to the relaxed eye, being focused at infinity. For a clear image of the microdisplay, with an adequate view of the surroundings, the FOV_A of the superlens is chosen to be $20° \pm 0.5°$. This has the view of the microdisplay span roughly 10% and 13% of the eye's horizontal FOV_A (210°) and vertical FOV_A (150°), respectively [16]. The second design criterion relates to the separation, s, between the principal planes of the plano-concave and plano-convex MLAs. It is desirable to have this separation be as small as possible, while leaving a gap of 25 μm to 50 μm between the MLAs to accommodate a baffle. The baffle takes the form of an array of microholes in a 25-μm-thick aluminum sheet, and it is used to block the light that passes between the microlenses. It has the same periodicity as the plano-concave MLA and it is butted up against this MLA. The third design criterion for the superlens relates to its

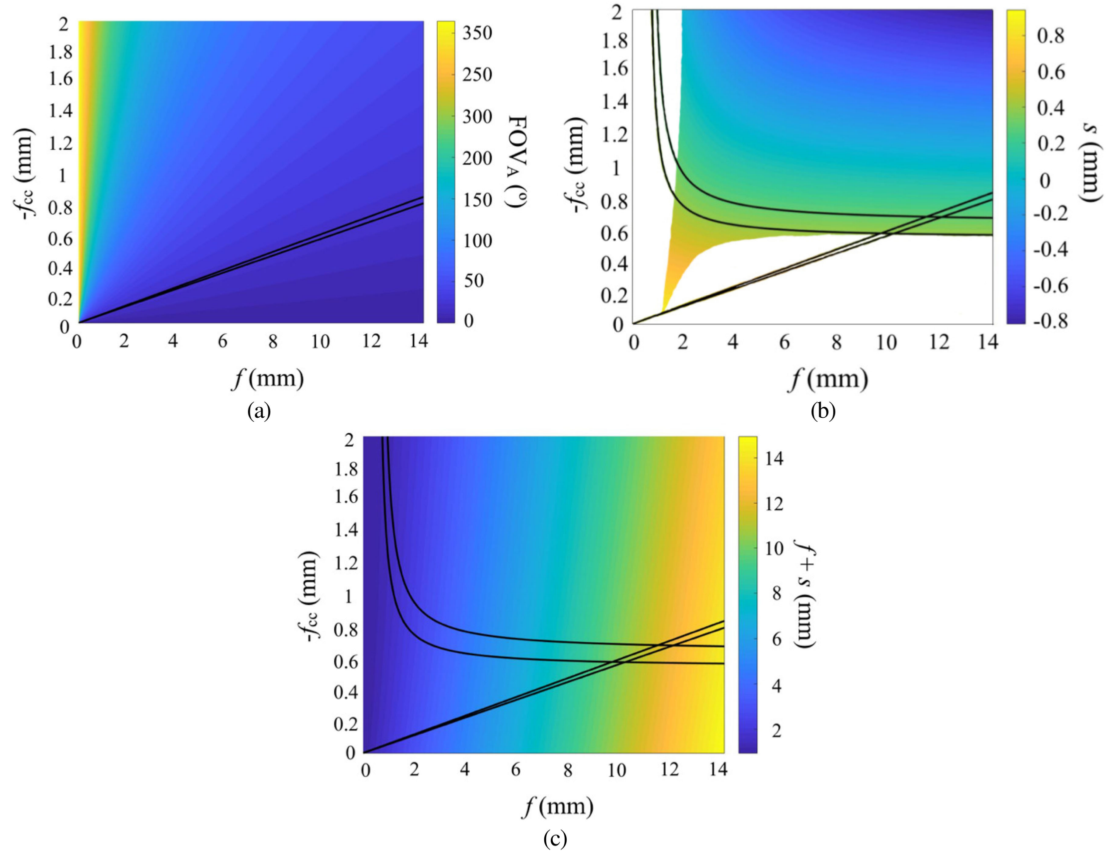

Fig. 2. **| Tradespace analyses to optimize the superlens.** (a) The superlens parameters are varied to optimize the FOV_A. (b) The superlens parameters are varied to optimize the separation, s, between the principal planes of the plano-concave and plano-convex MLAs. (c) The superlens parameters are varied to optimize the overall display length, $f + s$. The characteristics being optimized are shown as colourmaps versus the negated focal length of the plano-concave MLA, $-f_{cc}$, and the effective focal length between the microdisplay and the principal plane of the plano-concave MLAs, f. The linear band between black lines encloses values of $-f_{cc}$ and f that yield the desired FOV_A of $20° \pm 0.5°$. The curved band between black lines encloses values of $-f_{cc}$ and f that yield a separation, s, in the desired range from 365 μm to 390 μm.

need for a flat form factor. This criterion is met by simply minimizing the overall length of the display, being the sum of f and s.

Fig. 2(a) relates to the first design criterion, and it depicts the tradespace analysis for the FOV_A of the superlens. It is shown as a colourmap of the FOV_A versus the negated focal length of the plano-concave MLA, $-f_{cc}$, on the left axis, and the effective focal length between the microdisplay and plano-concave MLA, f, on the bottom axis. The FOV_A is defined as twice the maximum allowable angle off the optical axis for imaging by the relaxed eye, and it is given by $FOV_A = 2f_{cc}(3\text{ mm})180°/(f_{cv}(f - f_{cc})\pi)$, in degrees, where the dimension of 3 mm is half of the microdisplay's width. The linear band between the displayed black lines encloses values of $-f_{cc}$ and f that yield an FOV_A of $20° \pm 0.5°$, in accordance with the first design criterion. The linear trend of this band suggests that the desired FOV_A can be met by simply maintaining the ratio of these focal lengths at roughly $-f_{cc}/f \approx 0.058$.

Fig. 2(b) relates to the second design criterion, and it depicts the tradespace analysis for the separation, s, between the principal planes of the plano-concave and plano-convex MLAs. It is shown as a colourmap of this separation versus the negated focal length of the plano-concave MLA, $-f_{cc}$, on the left axis, and the effective focal length between the microdisplay and plano-concave MLA, f, on the bottom axis. Colours are not shown in the regions at the bottom and

TABLE 1
Optimized and Finalized Parameter Values for the Plano-Concave and Plano-Convex MLAs in the Superlens, in Terms of their Pitch, Diameter, Radius of Curvature (ROC), and Focal Length

	Pitch	Diameter	ROC	Focal length
Plano-concave MLA	$p_{cc} = 466\ \mu m$	$d_{cc} = 300\ \mu m$	$R_{cc} = 247\ \mu m$	$f_{cc} = -638\ \mu m$
Plano-convex MLA	$p_{cv} = 440\ \mu m$	$d_{cv} = 350\ \mu m$	$R_{cv} = 497\ \mu m$	$f_{cv} = 943\ \mu m$

left of this figure because the overall thickness of the microlens in these regions would need to be larger than its radius of curvature, and such a structure is unphysical. The figure displays the aforementioned linear band, between black lines, to designate the region of permissible values of the FOV_A. The figure also displays a curved band as the region that establishes a physical gap between the MLAs of 25 μm (corresponding to $s = 365$ μm and denoted by the top black line) to 50 μm (corresponding to $s = 390$ μm and denoted by the bottom black line), in accordance with the second design criterion. Ultimately, the region over which the linear and curved bands intersect identifies the values of $-f_{cc}$ and f that establish permissible values of the FOV_A and separation, s, between the principal planes of the MLA.

Fig. 2(c) relates to the third design criterion, and it depicts the tradespace analysis for the overall length of the display, $f + s$. It is shown as a colourmap of this length versus the negated focal length of the plano-concave MLA, $-f_{cc}$, on the left axis, and the effective focal length between the microdisplay and plano-concave MLA, f, on the bottom axis. The aforementioned regions of permissible FOV_A and s are displayed by way of the linear and curved bands, between black lines, respectively. It is apparent from the figure that the overall display length can be minimized, in accordance with the third design criterion, by choosing the smallest allowable effective focal length, being $f = 10$ mm. As a result, the separation between the principal planes of the plano-concave and plano-convex MLAs should be $s = 390$ μm, which gives a physical gap of 50 μm and a focal length for the plano-concave array of $f_{cc} = -638$ μm. The radius of curvature of the plano-concave MLA for this focal length can be estimated by using an algebraic (thin-lens) expression for f_{cc}, in the form of

$$f_{cc} = -\frac{R_{cc}}{n-1}, \tag{5}$$

where $n = 1.40$ is the refractive index of the underlying polydimethylsiloxane (PDMS) substrate. This gives a radius of curvature of $R_{cc} \approx 255$ μm. Note that this value is only an estimate because it is subject to the thin-lens approximation that is used to form equation (5). A more exact value for R_{cc} will be defined via the upcoming ray-based simulations.

To validate the findings of the tradespace analyses, and characterize the imaging performance without the underlying assumptions of ray transfer matrices, full ray-based simulations are carried out on the optimized superlens. Zemax OpticStudio software is used. In the simulations, each pixel on the microdisplay is treated as a point source of rays. The rays propagate through the coupled plano-concave and plano-convex MLAs and into the relaxed eye, within which they focus onto the retina. It is found that the values of all the parameters from the tradespace analyses of the superlens bring about the desired focusing on the retina—except for the estimated radius of curvature of the plano-concave MLA, which must be adjusted (slightly) to $R_{cc} = 247$ μm. All of the optimized and finalized parameter values are shown in Table 1.

The functionality of the developed superlens is shown in Fig. 3(a). The figure shows a cross-sectional view of light rays propagating away from the centre and outermost edges of the microdisplay, through the superlens, and onto the retina of the eye. It is apparent from this figure that the coupled MLAs can function as a superlens and effectively display images to the relaxed eye. The effectiveness of the superlens is defined by its resolution, which is quantified through the results shown in Fig. 3(b). The figure is created by displaying simulated test patterns on the

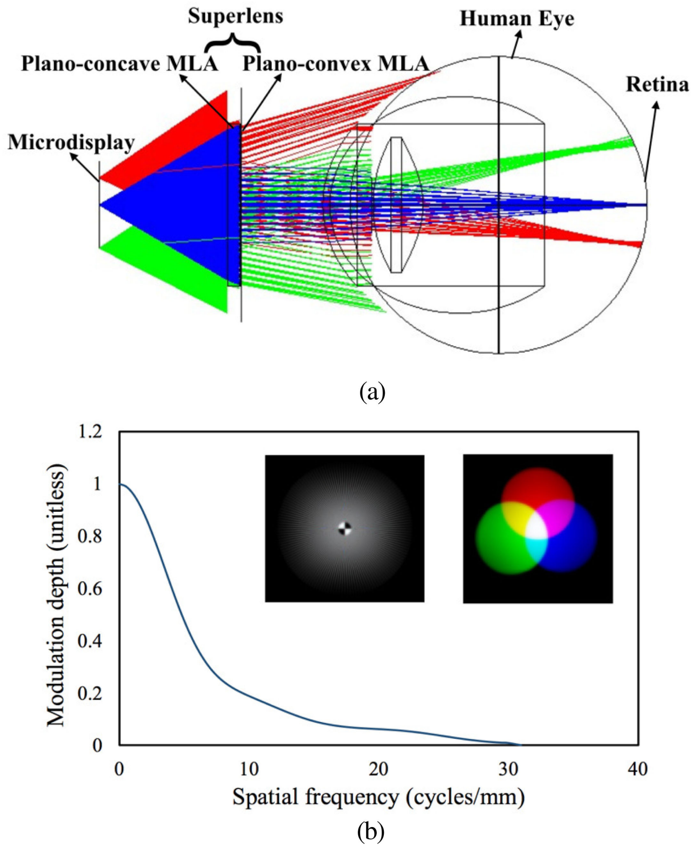

Fig. 3. **| Ray-based simulations for the optimized superlens.** (a) Light rays are shown emanating from the microdisplay, passing through the superlens, and focusing on the retina of the eye. (b) The resulting MTF of the superlens is shown as the modulation depth versus spatial modulation frequency. The insets of (b) display two representative colour photographs having been generated on the microdisplay, imaged by the superlens, and resolved on the retina of the eye.

microdisplay in the form of linear arrays with spatial modulation frequencies spanning 0 to 30 cycles/mm. The resulting images being resolved on the retina, for the various spatial modulation frequencies, are then analysed to define their ratios of highest to lowest intensities as modulation depths. The modulation depths for the entire range of spatial modulation frequencies establish the modulation transfer function (MTF) of the superlens [17]. The MTF of the simulated superlens is shown in the figure. (Since the coupled MLAs are symmetric, the tangential and sagittal responses are equivalent and are shown as one curve.) Two representative test images, having been generated on the microdisplay, imaged by the superlens, and resolved on the retina, are shown as insets. The results exhibit finite modulation depths up to 30 cycles/mm, which is indicative of strong imaging performance. The aberration that is present is attributed mainly to astigmatism, due to the rectangular (rather than radially-symmetric) distribution of microlenses in the MLAs, and spherical aberration, due to the non-ideal shape of the microlenses. According to Seidel diagrams collected from the ray-based simulations, not shown, the Seidel spherical aberration coefficients of the plano-concave and plano-convex MLAs are -2.28×10^4 and 4.79×10^3, respectively. Such spherical aberration could be reduced by future work in optimizing the microlens shapes.

3. Fabrication and Testing

The microlenses within the optimized superlens must be implemented with precise control over their diameters and radii of curvature, and a specialized fabrication process is developed to do this.

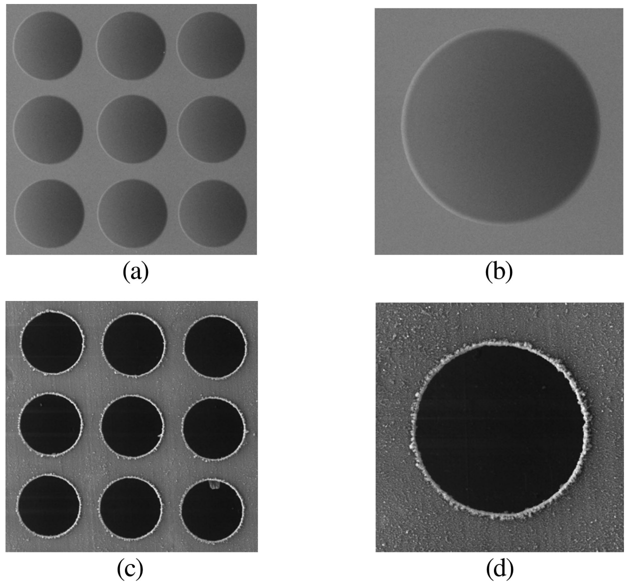

Fig. 4. **| SEM images of representative plano-convex microlenses and microholes within the baffle.** The displayed plano-convex microlenses and microholes have diameters of 367 μm and 330 μm, respectively.

The process starts with a plasma pre-treatment of a glass substrate, using a plasma treatment system (Plasma Etch PE-25) for a prescribed duration, to raise its surface energy and increase its wettability to polymer [12]. Polymer microdroplets are then dispensed and cured as arrays on the substrate. The arrays are used as is, to form the plano-convex MLA, or as a mold for casting [13], to form the plano-concave MLA. The MLAs are then coupled together, with the aforementioned baffle between them, to form the superlens. The baffle is an array of microholes having the same pitch as the plano-concave MLA. It is fabricated by a 355-nm laser micromaching system (Oxford Lasers Inc., A-series) having a 1-μm resolution. Scanning electron microscope (SEM) images of typical plano-convex MLAs and the baffle are shown in Fig. 4.

The microlens fabrication setup, used for dispensing and curing microlenses, is shown in Fig. 5(a). The setup dispenses microdroplets of Norland Optical Adhesive (NOA) 65 onto the 100-μm-thick glass substrate via a 32-gauge needle tip using a precision dispenser (Nordson EFD Ultimus V). The ensuing ultraviolet (365-nm) curing is applied by an optical fibre. The necessary level of reproducibility is achieved by LabVIEW-based control for the dispensing, curing, and actuation, with a motorized xyz-translation stage (Thorlabs PT3-Z8). Tunability is realized by adjusting the dispensing pressure and time, with increased pressures and times yielding increased microlens diameters. The fabrication process was fully characterized and found to reliably form microlenses with diameters from 200 μm to 400 μm and radii of curvature from 200 μm to 700 μm, with deviations of less than 2% across a typical array. (It was noted through such characterizations that great care should be paid to leveling the substrate prior to dispensing in order to achieve this 2% tolerance across a given MLA.) Ultimately, the microlens fabrication setup was applied to the fabrication of two arrays of plano-convex microlenses.

The first fabricated array is used as the plano-convex MLA within the superlens. It was formed on a 100-μm-thick glass substrate having undergone a plasma pre-treatment at a power of 22.5 W over a time of 10 s, and its microlenses were formed with a dispensing pressure of 9.5 psi and dispensing time of 250 ms. This yielded a plano-convex MLA with microlenses having a pitch of (440 ± 2.0) μm, diameter of (350 ± 6.87) μm, and radius of curvature of (497 ± 9.81) μm. These values are within tolerance of the optimized design parameters in Table 1.

The second fabricated array is used as a mold to cast the plano-concave MLA within the superlens. It was formed on a 100-μm-thick glass substrate that did not undergo a plasma pre-treatment.

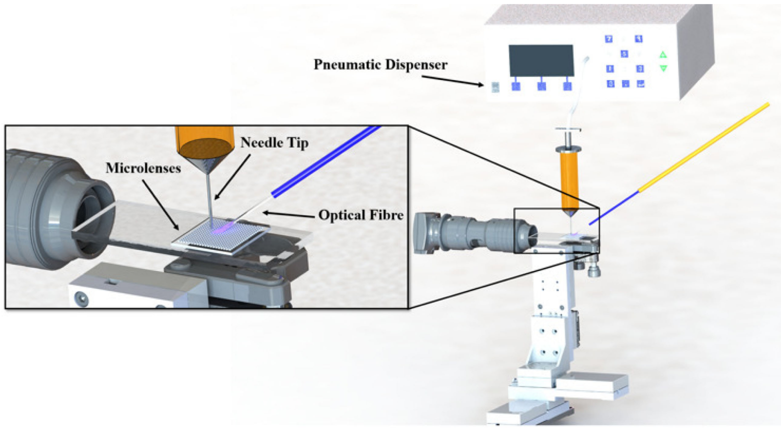

(a)

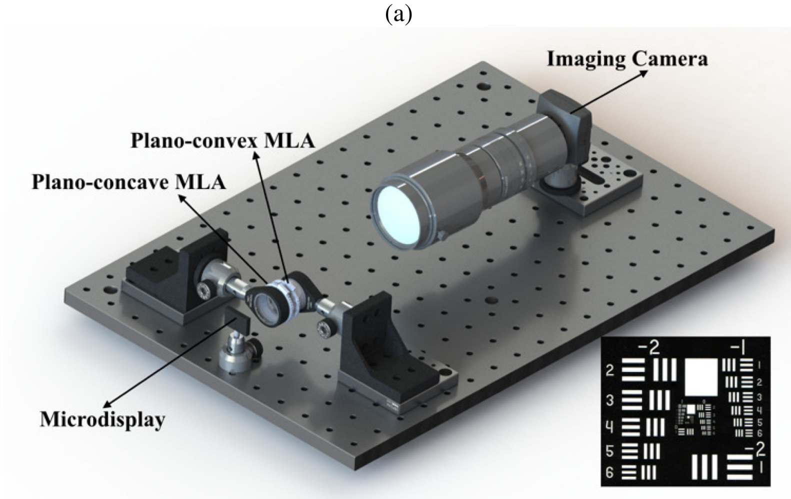

(b)

Fig. 5. | **Experimental schematics.** (a) A schematic is shown of the microlens fabrication setup that dispenses/cures microlenses. (b), A schematic is shown of the imaging setup used to characterize the performance of the coupled MLAs in the superlens.

(The pre-treatment was not necessary to achieve the parameters needed for this array.) Its microlenses were formed with a dispensing pressure of 7.5 psi and dispensing time of 200 ms. This yielded a plano-convex MLA that was used as a mold for casting into PDMS. The PDMS had a ratio of resin to curing agent of 5 to 1, given that this ratio was found to yield enhanced flexibility. The PDMS was then baked in an oven at a temperature of 60° for 36 minutes and cooled to room temperature over one hour. The cured PDMS was then peeled off the mold to release the plano-concave MLA. The resulting plano-concave MLA had microlenses with a pitch of (466 $\pm$ 2.0) μm, diameter of (300 $\pm$ 5.89) μm, and radius of curvature of (247 $\pm$ 4.85) μm. Such values are within tolerance of the optimized design parameters in Table 1.

The plano-concave and plano-convex MLAs were coupled as a superlens for testing. The MLAs were separated by the aforementioned gap of 50 μm and rotated, as needed, to align the rows and columns of microlenses. The alignment became optimal when the number of Moiré patterns was minimized. The superlens was then packaged with the microdisplay, to form the heads-up display, and its performance was analysed with the imaging setup shown in Fig. 5(b). The setup uses an imaging camera with a sufficiently high resolution and variable focus, from zero to infinity, to act as the human eye. Test patterns were generated on the microdisplay, in the form of linear arrays with spatial modulation frequencies spanning 0 to 30 cycles/mm, and images of the patterns

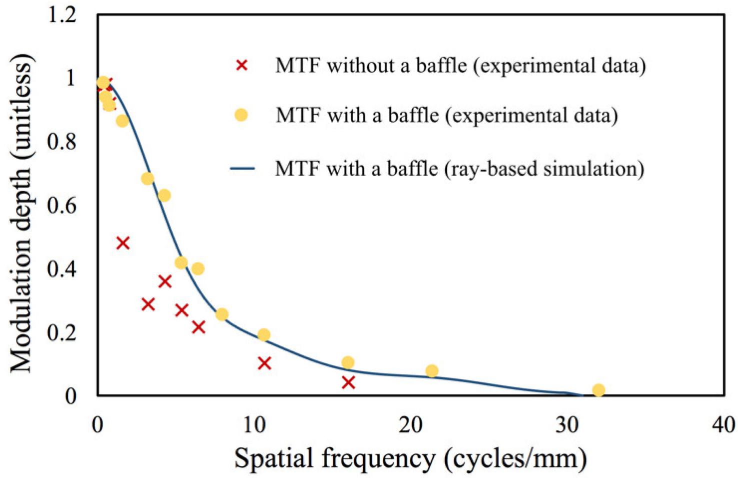

Fig. 6. | **Modulation depth versus spatial frequency, defining the MTF.** Experimental data points are shown for the optimized superlens without a baffle (red crosses) and the optimized superlens with a baffle (solid yellow circles). A theoretical curve from ray-based simulations is shown for the optimized superlens with a baffle (solid blue line).

were captured by the camera. The modulation depths in the images, for differing spatial modulation frequencies, were extracted to generate the MTF of the superlens.

The superlens was tested in two configurations—being with and without the baffle in the central 50-μm gap. The MTF results of the superlens with and without the baffle are shown in Fig. 6 by way of red crosses and solid yellow circles, respectively. The figure also shows the MTF results from ray-based simulations of the superlens with a baffle as a solid blue curve. It is apparent from the results that experimental and theoretical results for the superlens with the baffle show good agreement. It is also apparent that the baffle plays an important role in blocking light that passes between the microlenses, which would otherwise blur the image, and transmitting light that passes through the microlenses, which resolves the image of the microdisplay. Ultimately, the superlens without the baffle yields a maximum MTF of 16 cycles/mm, while the superlens with the baffle yields a maximum MTF of 30 cycles/mm. The later result is indicative of strong imaging performance.

4. Conclusion

In conclusion, the proposed work targeted the fundamental challenge of heads-up display technologies, which demand tight imaging and a sufficiently flat form factor for integration within eyewear. A Gabor superlens, with coupled plano-concave and plano-convex MLAs, was developed in this effort. Tradespace analyses and ray-based simulations were used to design the MLAs and optimize their parameters for use in the superlens. The MLAs were then formed by a specialized fabrication process that applied plasma pre-treatment and microlens dispensing, curing, and casting to create the microlenses with the necessary diameters and radii of curvature for the MLAs. The fabricated plano-concave and plano-convex MLAs were coupled as a superlens and packaged with a baffle and microdisplay to function as a heads-up display. Theoretical and experimental characterizations of the display exhibited strong imaging performance, with a resolution of up to 30 cycles/mm. Such findings can lay the groundwork for emerging heads-up display technologies.

Acknowledgement

This work was carried out through a partnership between researchers at the University of British Columbia and Intel Corporation. The SOLIDWORKS schematic of the human eye in Fig. 1 was created by S. White and was used with permission.

References

[1] S. R. Soomro and H. Urey, "Light-efficient augmented reality 3D display using highly transparent retro-reflective screen," *Appl. Opt.*, vol. 56, pp. 6108–6113, 2017.
[2] S. Pleasant, "Displays: Wide-angle head-up display," *Nat. Photon.*, vol. 8, no. 84, pp. A121–A124, 2014.
[3] D. Cheng, Y. Wang, H. Hua, and J. Sasian, "Design of a wide-angle, light-weight head-mounted display using free-form optics tiling," *Opt. Lett.*, vol. 36, pp. 2098–2100, 2011.
[4] C. Hemdb-Sölner, R. F. Stevens, and M. C. Hutley, "Imaging properties of the Gabor Superlens," *J. Opt. A, Pure Appl. Opt.*, vol. 1, pp. 94–102, 1999.
[5] N. F. Borrelli, R. H. Bellman, J.A. Durbin, and W. Lama, "Imaging and radiometric properties of microlens arrays," *Appl. Opt.*, vol. 30, pp. 3633–3642, 1991.
[6] D. Gabor, "Improvements in or relating to optical systems composed of lenticules," U.K. Patent 541,753, Dec. 10, 1941.
[7] W. Choi, R. Shin, J. Kim, and S. Kang, "Design methodology for a confocal imaging system using an objective microlens array with an increased working distance," *Sci. Rep.*, vol. 6, 2016 , Art. no. 33278.
[8] W. J. Hossack, E. Theofanidou, J. Crain, K. Heggarty, and M. Birch, "High-speed holographic optical tweezers using a ferroelectric liquid crystal microdisplay," *Opt. Exp.*, vol. 11, pp. 2053–2059, 2003.
[9] M. E. Jungwirth, D. V. Wick, and E. L. Dereniak, "Theory and tradespace analysis of a reflective axial adaptive optical zoom system," *Opt. Eng.*, vol. 51, 2012, Art. no. 083001.
[10] N. G. Douglas, A. R. Jones, and F. J. V. Hoesel, "Ray-based simulation of an optical interferometer," *J. Opt. Soc. Amer. A*, vol. 12, pp. 124–131, 1995.
[11] S. Ha, H. Yu, N. Jiang, J. H. Kim, S. Kim, and J. Kim, "Compact and high-power dye-sensitized solar system integrated with low-cost solar-concentrating polymer lens," *Sol. Energy Mater. Sol. Cells*, vol. 155, pp. 362–367, 2016.
[12] R. Wang, Y. Shen, C. Zhang, P. Yan, and T. Shao, "Comparison between helium and argon plasma jets on improving the hydrophilic property of PMMA surface," *Appl. Surf. Sci.*, vol. 367, pp. 401–406, 2016.
[13] E. A. Travnicek, "Contact lens casting method," U.S. Patent 4 141 941A, Feb. 27, 1979.
[14] N. Lindlein, "Simulation of micro-optical systems including microlens arrays," *J. Opt. A, Pure Appl. Opt.*, vol. 4, pp. S1–S9, 2002.
[15] K. Lee and Y. Park, "Exploiting the speckle-correlation scattering matrix for a compact reference-free holographic image sensor," *Nature Commun.*, vol. 7, 2016, Art. no. 13359.
[16] K. K. Ball, B. L. Beard, D. L. Roenker, R. L. Miller, and D. S. Griggs, "Age and visual search: Expanding the useful field of view," *J. Opt. Soc. Amer. A*, vol. 5, pp. 2210–2219, 1988.
[17] S. K. Park, R. Schowengerdt, and M.-A Kaczynski, "Modulation transfer function analysis for sampled image systems," *Appl. Opt.*, vol. 23, pp. 2572–2582, 1984.
[18] H. S. Park, R. Hoskinson, H. Abdollahi, and B. Stoeber, "Compact near-eye display system using a superlens-based microlens array magnifier," *Opt. Exp.*, vol. 23, pp. 30681–30633, 2015.